J Solid State Electrochem (2012) 16:2581–2590
DOI 10.1007/s10008-012-1664-0

ORIGINAL PAPER

Lithium electrochromism of atmospheric pressure plasma jet-synthesized NiO_xC_y thin films

Yung-Sen Lin · Di-Jiun Lin · Lu-Yan Chiu · Sheng-Wei Lin

Received: 13 November 2011 / Revised: 17 January 2012 / Accepted: 21 January 2012 / Published online: 18 February 2012

Abstract Reversible lithium intercalation and deintercalation behavior of atmospheric pressure plasma jet (APPJ)-synthesized organonickel oxide (NiO_xC_y) thin films under various substrate distances is testified in an electrolyte (1 M $LiClO_4$–propylene carbonate solution) at low driving voltages from −0.5 to 1.5 V. Fast responses of 2 s bleaching at −0.5 V and 6 s coloration at +1.5 V are accomplished for the nano-porous NiO_xC_y thin films. This study reveals that a rapid synthesis of electrochromic NiO_xC_y thin films in a single process via APPJ by 21 s is investigated. This study presents a noteworthy electrochromic performance in a light modulation with up to 43% of transmittance variation and a coloration efficiency of 36.3 cm^2/C at a wavelength of 830 nm after 200 cycles of cyclic voltammetry measurements.

Keywords Atmospheric plasma · Plasma jet · PECVD · Electrochromism · Nickel oxide

Introduction

For electrochromic devices (ECDs) to make use of automotive (glazing of sunroofs, windows, and mirrors), architectural (energy efficient glazing (smart switchable windows), privacy glass, partitions, and skylights), and informational display industries, electrochromic nickel oxides (NiO_x) thin films are the most frequently used anodic oxide-based electrochromic materials to complementary to cathodic–electrochromic tungsten oxides (WO_x) thin films [1]. Electrochromism of NiO_x films in electrolytes has been intensively investigated in the last two decades, but issues still remain with respect to scale-up and poor stability in aqueous basic media [2]. Passerini et al. [3] testified that direct current (d.c.)-sputtered nickel oxide (NiO_x) films undergo a reversible lithium intercalation–deintercalation process, which is accompanied via a net electrochromic effect by the following electrochemical process in a non-aqueous lithium containing electrolyte (1):

$$\mathrm{Li}_{\alpha_0}\mathrm{NiO}_x\ (\text{colored}) + \alpha_i \mathrm{Li}^+ + \alpha_i \mathrm{e}^- \underset{\text{coloring}}{\overset{\text{bleaching}}{\rightleftharpoons}} \mathrm{Li}_{(\alpha_0+\alpha_i)} \left[\mathrm{Ni}^{3+}_{1-\alpha_i}\mathrm{Ni}^{2+}_{\alpha_i}\right]\mathrm{O}_x\ (\text{bleached}) \quad (1)$$

Once electrochromic NiO_x film can be synthesized via vapor deposition method with a rapid single process and a low moisture ambient, then the issues regarding scale-up and irreversible water trapped in the films can be solved. Electrochromic nickel oxide films have been deposited by a variety of methods, including sol–gel deposition [4], electrodeposition [5], spray pyrolysis [6], evaporation [7], sputtering [8], and laser ablation deposition [9]. For vapor deposition methods, sputtering is usually employed for nickel oxide film deposition. Plasma-enhanced chemical vapor deposition (PECVD) has not yet investigated for synthesis of nickel oxide thin films, although PECVD provides higher deposition rates than sputtering, results in lower cost for depositing of oxide films by PECVD in a factor of 3 lower than that for sputtering (the cost was calculated for the size of glass substrate at 2×3 m) [10]. This study attempts to deal with rapid depositions of electrochromic NiO_xC_y films onto glass/ITO substrates using atmospheric pressure (AP)-PECVD with atmospheric pressure plasma jet (APPJ) by short durations of 21–28 s exposed in plasmas. Corona discharge, dielectric barrier discharge

Y.-S. Lin (✉) · D.-J. Lin · L.-Y. Chiu · S.-W. Lin
Department of Chemical Engineering, Feng Chia University,
No.100, Wenhwa Rd., Seatwen,
Taichung, Taiwan 40724, Republic of China
e-mail: yslin@fcu.edu.tw

(DBD), and APPJ are the typical cold atmospheric plasma sources. Corona discharge causes unstable plasma densities and is not likely to deposit thin films. Small discharge gap (typical 2~5 mm) between electrodes are required for DBD, which limits the substrate thickness and the shape of substrate for thin film deposition. In this study, APPJ is investigated to deposit electrochromic NiO_xC_y films by reason of APPJ not limits the substrate thickness and the shape of substrate by locating the substrates on the downstream of plasma jet. Low-temperature AP-PECVD process with a precursor NO vapor carried by argon gas, mixed with oxygen gas, and then injected into air plasma jet to deposit electrochromic NiO_xC_y films onto moving glass/ITO substrates is examined. This study investigates how the process parameter, namely the substrate distances, influences the film properties and the electrochromic performance of APPJ-synthesized NiO_xC_y films. The nature of NiO_xC_y films is examined by field emission scanning electron microscopy (FESEM), Raman spectroscopy, and X-ray photoelectron spectroscopy (XPS).

Experimental details

Synthesis of NiO_xC_y films via APPJ

The schematics of the APPJ setup for deposition of NiO_xC_y films onto the glass/ITO substrates (15 Ω/square, 1.1 mm thick, 3×4 cm) in air are shown in Fig. 1. The air plasma torch of the APPJ is generated by an atmospheric pressure non-equilibrium glow discharge with a power supply at an audiofrequency of 20 kHz and a power of 300 W. The precursor [nickelocene, $Ni(C_5H_5)_2$; NO] powders are put in a sublimator and heated at 140 °C. Then, 4.1 sccm of Ar gas (99.9% pure) is fed into the tank to carry 9.4 sccm of NO vapor and mixed with 7.9 sccm of oxygen gas (99.9% pure) (the gas line is heated at 140 °C) for injection into air plasma torch at an angle of 15° with respect to the nozzle. The glass/ITO substrates are mounted 1.4–2.0 cm below the nozzle of the air plasma torch. The film-formable reactive species in plasmas are applied onto the surface of glass/ITO substrate at a substrate moving speed of 8 cm/s for synthesis of NiO_xC_y films. Other settings are shown in Table 1. The glass/ITO substrates are exposed directly to the plasmas for 21–28 s to reduce the thickness variation to be less than 5%. Then, the glass/ITO/NiO_xC_y is taken for measurements within 30 min under the temperature at ~23±1 °C and the relative moisture at ~40±5%. In this study, experiments are repeated five times. The variation in experiments between the prepared samples is controlled at less than 10%.

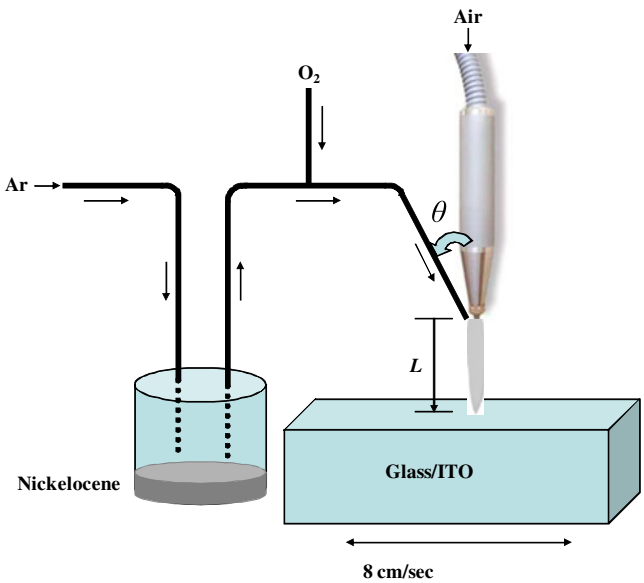

Fig. 1 Schematics of the APPJ setup for deposition of NiO_xC_y films onto glass/ITO substrates

Thin film analysis

Surface morphology and thickness of NiO_xC_y films are examined from the top surfaces and cross sections of the specimen by FESEM. The porosity on the surface of each sample is interpreted by the grain boundary fraction (in percent) of FESEM image on the top surface. A high grain boundary fraction (in percent) refers to high porosity. The grain boundary fraction (in percent) on the surface of each sample is calculated by dividing the area of grain boundary by the total area of coatings on the FESEM images using the Image-Pro Plus-Version 4.5.0.29 software (purchased from Media Cybermetics, Inc). Deposition rates of APPJ-synthesized NiO_xC_y film are determined by film thickness (from FESEM image on the cross section) divided by the duration of deposition. FESEM images are collected on a HITACHI S-4800. The system equipped with an electron gun emitting a cold field with an electrical voltage of 1 kV and an electrical current of 5 μA. Data are recorded for a scan area of 500×500 nm^2 with 1,024×840 pixels.

Table 1 The settings for deposition of NiO_xC_y films onto glass/ITO substrates by APPJ

Parameters	Settings		
Power (W)	300		
Frequency (kHz)	20		
Air flow rate (l/min)	33.3		
Ar flow rate (sccm)	4.1		
O_2 flow rate (sccm)	7.9		
Nickelocene flow rate (sccm)	9.4		
Precursor injection angle θ (°)	15		
Substrate moving speed (cm/s)	8		
Substrate distance L (cm)	1.4	1.7	2.0
Exposed duration (s)	21	22	28

Raman spectra of the specimen are collected by a Renishaw inVia Raman spectrometer with a magnitude of ×50 microscope. A diode type of Ar^+ laser of wavelength 785 nm is used. Data are recorded at an Ar^+ laser beam focused on a spot of 5 × 5 μm^2 in size. A lower power of about 1.4 mW is applied to avoid local heating of the specimen. Raman shifts between the wavenumbers 200 and 1,900 cm^{-1} are measured.

The XPS spectra of the specimen are collected by a Thermo VG Scientific Sigma Probe system, which is equipped with an Al Kα X-ray monochromatic source at 1,486.6 eV and charge compensation of 0.4 mA to compositionally analyze samples. Survey scans at the low-resolution mode with an analyzer pass energy of 5 eV and multiplex (narrow) scans at the high-resolution mode with an analyzer pass energy of 50 eV are taken. Data are recorded at a 53° collecting angle. The high-resolution spectra have a spot size of 400×400 μm^2 and an analysis depth of ~5 nm. The following NiO_x coating binding energies are analyzed: $Ni^{2+}_{2p3/2}$ and $Ni^{3+}_{2p3/2}$ of Ni_{2p} at 854.5 and 856.5 eV; NiO, Ni_2O_3, C=O, and C–O of O_{1s} at 529.5, 531.5, 531.8, and 532.0 eV; and C–C, C–O, and C=O of C_{1s} at 284.4, 286.1, and 288.4 eV, respectively [11, 12].

Electrochromic characterization

A three-electrode electrochemical system (Jiehan 5000) with the potential sweep method (Li^+ intercalation from 1.5 to −0.5 V at a scan rate of −50 mV/s and Li^+ deintercalation from −0.5 to 1.5 V at a scan rate of 50 mV/s are set), and the potential step method (at −0.5 V for 10 s and at 1.5 V for 10 s) is used to evaluate the Li^+ intercalation and deintercalation behaviors of NiO_xC_y films. The glass/ITO/NiO_xC_y is mounted on a working electrode. The Pt grid and Ag/AgCl are used as the counter electrode and reference electrode, respectively. All potential values in this study are applied versus the standard hydrogen potential. The electrolyte is a 1-M $LiClO_4$-PC solution, which is placed in a dry box. A glass cell filled with the electrolyte is taken as the background. The in situ spectroelectrochromic performance of NiO_xC_y films is recorded with potentiostat/galvanostat (Jiehan 5000) and spectrophotometer (Labguide DH2000-BAL).

Electrochromic performance of glass/ITO/APPJ-synthesized NiO_xC_y is determined in terms of transmittance variation (ΔT), optical density change (ΔOD), and color efficiency (η) by Eqs. 2–4:

$$\Delta T(\%) = T_{\text{bleached}}(\%) - T_{\text{colored}}(\%) \tag{2}$$

$$\Delta \text{OD} = \log\left[\frac{T_{\text{bleached}}(\%)}{T_{\text{colored}}(\%)}\right] \tag{3}$$

$$\eta = \frac{\Delta \text{OD}}{q} \tag{4}$$

where T_{bleached} (in percent) and T_{colored} (in percent) denote the transmittance of the specimen in the bleached state (ion intercalation state) and colored state (ion deintercalation state), respectively, and q denotes the charge intercalation/deintercalation per unit area.

Intercalation coefficient α_i and deintercalation coefficient α_d

The quantity α_i (α_d) is termed as the Li^+ intercalation coefficient (deintercalation coefficient) of $Li_{\alpha_i}NiO_xC_y$ ($Li_{\alpha_i-\alpha_d}NiO_xC_y$) in Eq. 5 and depends on the charge passed, hence on the extent of electrode reaction. It can be estimated by Eqs. 5–7:

$$\alpha_i; \alpha_d = \frac{M_{Li^+}}{M_{NiO_xC_y}} \tag{5}$$

$$M_{Li^+} = \frac{\left(\frac{q}{q_{e^-}}\right)}{N} \tag{6}$$

$$M_{NiO_xC_y} = \frac{V \times \rho}{m} \tag{7}$$

where M_{Li^+} is the moles of lithium ions intercalated (deintercalated), $M_{NiO_xC_y}$ is the moles of Ni oxide deposited, V is the film volume, ρ is the film density (which is obtained by the film's weight divided by the film's volume, the film's volume is calculated by the film's area multiples the thickness of the film), m is the atomic weight of the Ni oxide, q is the Li^+ intercalated (deintercalated) charge, q_{e^-} is the charge of an electron, and N is Avogadro's number.

Results and discussion

Surface morphology, deposition rate, and film properties

The nano-porous surfaces of glass/ITO/NiO_xC_y films are remarked on the FESEM images of NiO_xC_y films while synthesized using APPJ at substrate distances of 1.4–2.0 cm, as shown in Fig. 2a–c. The porosity on the top surfaces of NiO_xC_y films can be illustrated in Table 2 as the ranking of the grain boundary fraction ε (in percent) dependent on the substrate distances: $\varepsilon_{1.4\text{ cm}}(13.8\%) >> \varepsilon_{2.0\text{ cm}}(5.7\%) > \varepsilon_{1.7\text{ cm}}(4.2\%)$. This indicates that the shorter the substrate distance at 1.4 cm for deposition of NiO_xC_y films, the more porous the surfaces of NiO_xC_y films. The substrates at 1.7 and 2.0 cm show the comparable porous surfaces.

Table 2 shows the thicknesses and the deposition rates of NiO_xC_y films deposited onto glass/ITO substrate at various

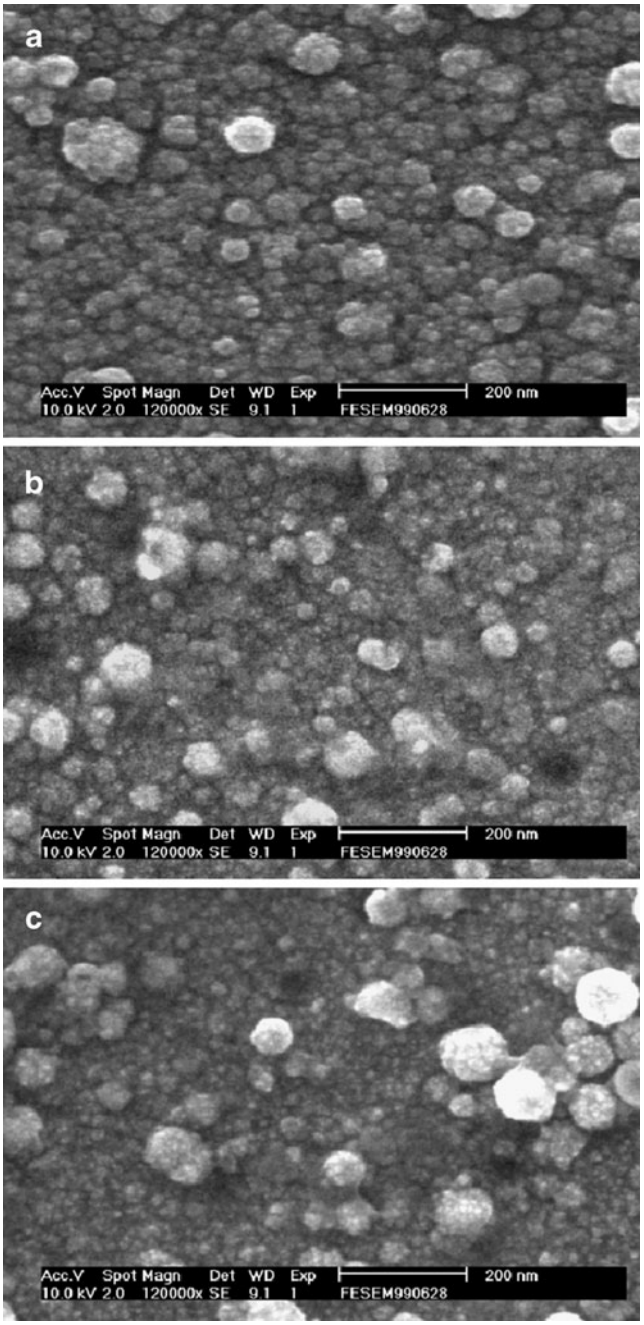

Fig. 2 FESEM images of glass/ITO/NiO_xC_y prepared at substrate distances of **a** 1.4 m, **b** 1.7 cm, and **c** 2.0 cm

Table 2 Grain boundary fraction, thickness, and deposition rate of APPJ-synthesized NiO_xC_y films onto glass/ITO substrates at various substrate distances

Substrate distance (cm)	Grain boundary fraction (%)	Thickness (nm)	Deposition rate (nm/s)
1.4	13.8	262±13.1	12.5±0.6
1.7	4.2	253±12.7	11.4±0.6
2.0	5.7	252±12.6	8.9±0.4

substrate distances via APPJ. The thicknesses of NiO_xC_y films coated at the substrate distances of 1.4–2.0 cm are 252–262 nm. This confirms that the thickness variation is less than 4%. The highest deposition rate (12.5 nm/s) of NiO_xC_y film is achieved at the lower substrate distance of 1.4 cm. Magnetron sputtering has commonly been used for deposition of electrochromic NiO_x films [1]. Estrada et al. reported that too high sputter rates of NiO_x films could lead to films that are incapable of extended color/bleach cycling in electrochromic devices [13]. A high deposition rate of up to ~2 nm/s for sputtered electrochromic NiO_x films has been testified by Wruck et al. [14]. Therefore, this study shows a high-rate deposition (up to of 12.5 nm/s) of electrochromic NiO_xC_y thin film onto glass/ITO substrate using APPJ. The existence of large populations of energetic electrons permits efficient, non-thermal dissociation of molecular gases or other vapor precursors to create high concentrations of reactive radical species that are typically observed in cold atmospheric plasmas [15]. In this study, precursor [nickelocene, $Ni(C_5H_5)_2$] is injected into air plasma torch; the reactive radical species such as $\bullet Ni \bullet$, $O \bullet$, $\bullet C \bullet$, $N \bullet$, and $H \bullet$ are generated. Hence, the reactive radical species such as $\bullet Ni \bullet$, $O \bullet$, and $\bullet C \bullet$ spray onto substrate and react to form NiO_xC_y thin film. However, the radical species $H \bullet$, $N \bullet$, and $O \bullet$ spray onto substrate and react to produce chemical bonds O–H and O–N. The chemical bonds O–H and O–N are not attached to substrate and sprayed out from substrate. Therefore, the chemical bonds O–H and O–N do not incorporate in deposition of NiO_xC_y thin film; results in the atomic compositions of N and H are negligible in NiO_xC_y thin film. Although carbon does not entail the Li^+ intercalation into and deintercalation out from NiO_xC_y thin film, the reactive radical species $\bullet C \bullet$ in the plasmas assist the reactive species $\bullet Ni \bullet$ and $\bullet O \bullet$ co-synthesized to fabricate NiO_xC_y thin film. In this study, the depositions of the electrochromic NiO_xC_y films onto glass/ITO substrates using APPJ go along with the step growth routes to generate fast deposition rates due to the reactive radical species. The FESEM images in Fig. 2a–c reveal the depositions of the electrochromic NiO_xC_y films onto glass/ITO substrates using APPJ formation of agglomerated nano-particles from the reactive radical species, which refers to the nucleation mechanism in a recent review by Borra [16]. Two types of metal oxide nanostructures such as spherical nano-particles and flat nano-sheets dependent on the substrate distances from the nozzle of the atmospheric pressure microplasmas have been described by Mariotti and Ostrikov [17]. In this study, only one type of nano-architecture is made up of spherical nano-particles for NiO_xC_y nano-structure is produced.

Raman spectra for NiO_xC_y films synthesized by APPJ at various precursor injection angles are shown in Fig. 3. Three broad peaks centered at 505, 1,356, and 1,540 cm^{-1} are

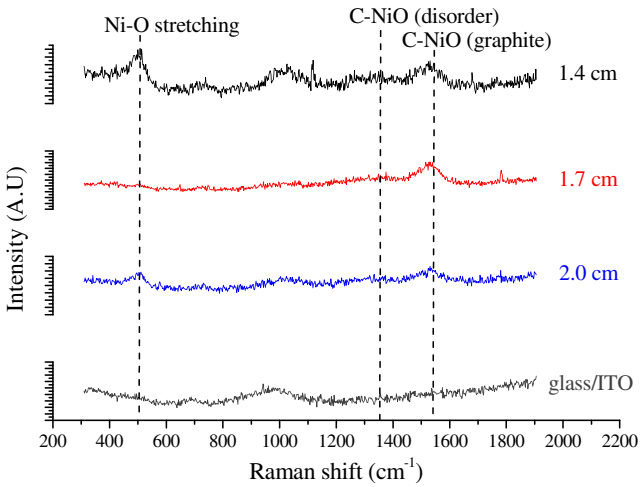

Fig. 3 Raman spectra of glass/ITO substrate and glass/ITO/NiO_xC_y at various substrate distances

illustrated in APPJ-synthesized NiO_xC_y films, respectively. The Ni–O stretching mode at 505 cm^{-1} [18], C–NiO stretch mode for the disorder carbon-bonded NiO at 1,356 cm^{-1}, and C–NiO stretch mode for the perfect graphite-bonded NiO at 1,540 cm^{-1} [19] have been assigned in Table 3, respectively. Figure 3 indicates that the lower the precursor injection angle, the higher the intensities of the peak for the perfect graphite-bonded NiO and the higher the intensities of the peak for Ni–O stretching.

Figure 3 indicates that Ni–OH stretching mode (~455 cm^{-1}) and Ni–O vibration mode (~490 cm^{-1}) for $Ni(OH)_2$ are not observed in APPJ-synthesized NiO_xC_y films [20]. The bands at ~530 cm^{-1} for NiOOH [21] and ~1,691 cm^{-1} for Ni–H stretching mode [22] are not detected in APPJ-synthesized NiO_xC_y films. In this study, the nickel oxides such as NiOOH and Ni$(OH)_2$ are not involved in the bleaching and coloring of APPJ-synthesized NiO_xC_y films in a 1-M $LiClO_4$–PC solution.

Potential sweep electrochromism

Green et al. [23] report that NiO_x thin films have better reversibility in a lithium containing electrolyte 1-M $LiClO_4$–PC than in aqueous-based electrolytes such as 1 M KOH and 0.1 M propionic acid. Figure 4a–d shows the cyclic voltammograms of NiO_xC_y thin films at substrate distances of 1.4–2.0 cm after Li^+ intercalation from 1.5 to −0.5 V at a scan rate of −50 mV/s and deintercalation from −0.5 V to 1.5 V at a scan rate of 50 mV/s in a 1-M $LiClO_4$–PC electrolyte for

Table 3 Results of Raman analyses for glass/ITO/NiO_xC_y

Peak position (cm^{-1})	Assignment
505	Ni–O stretching
1,356	C–NiO (disorder carbon)
1,540	C–NiO (disorder carbon)

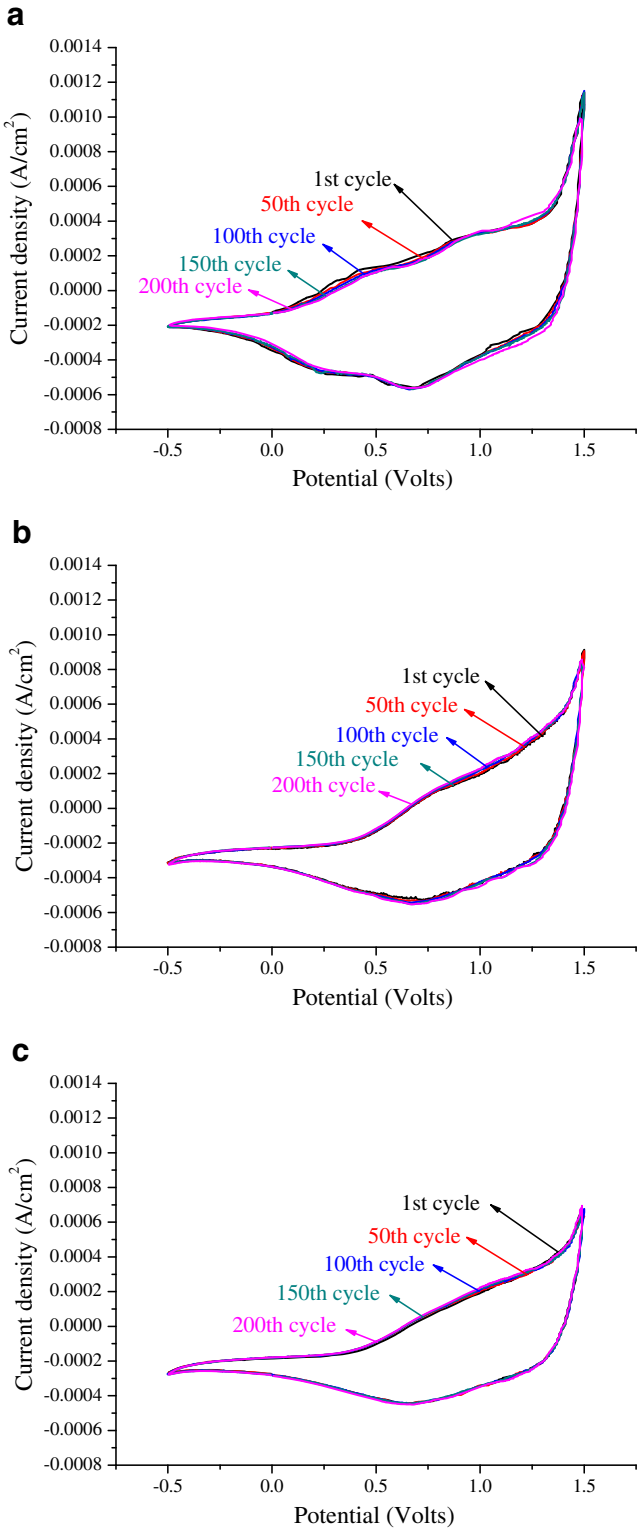

Fig. 4 Cyclic voltammograms of glass/ITO/NiO_xC_y after 1–200 cycles of Li^+ intercalation and deintercalation for substrate distances of **a** 1.4 cm, **b** 1.7 cm, and **c** 2.0 cm

200 cycles. Figure 4a–d indicates that the excellent reversibility of Li^+ intercalation into and deintercalation out from NiO_xC_y thin films is demonstrated for the negligible

differences of cyclic voltammograms after 1–200 cycles of cyclic voltammetry (CV) measurements.

The main advantages for ECDs are the efficiency in rejecting solar heat gains and admitting daylight. Low-voltage power is involved to switch, and no power is expected to keep up the ECDs in colored or bleached states. Consequently, the transmittances not only in the visible light region at wavelengths 400–700 nm but also in the infrared region at wavelengths 700–900 nm are investigated in this study. Figure 5 shows the transmittance spectra of as-deposited, the bleached, and colored glass/ITO/NiO_xC_y after 200 cycles of CV measurements at the wavelengths of 400–900 nm. Figure 5 indicates that the lower the substrate distance for NiO_xC_y films, the wider the wavelength ranges of the same transmittances for as-deposited and colored NiO_xC_y films. The equal transmittances for as-deposited and colored NiO_xC_y films are at the wavelengths of 400–900, 400–685, and 545–695 nm for the substrate distances at 1.4, 1.7, and 2.0 cm, respectively. Figure 5 reveals that the lower the substrate distance L (centimeters), the higher the transmittance spectra at bleached state T_b (in percent) and the lower the transmittance spectra at colored state T_c (in percent) of glass/ITO/NiO_xC_y. For NiO_xC_y thin film synthesized at the lower substrate distance of 1.4 cm, T_b (in percent) of 84.7% and T_c (in percent) of 46.3% at a wavelength of 550 nm and T_b (in percent) of 93.1% and T_c (in percent) of 50.1% at a wavelength of 830 nm are achieved, resulting transmittance variation ΔT of 38.4% and 43.0% at wavelengths of 550 and 830 nm, respectively.

In this study, electrochromic performance of glass/ITO/NiO_xC_y is illustrated by transmittance variation ΔT, optical density change ΔOD, and color efficiency η as a function of wavelength (400–900 nm) after 200 cycles of CV measurements, as shown in Fig. 6a–c. The lower the substrate distance L (centimeters) from the nozzle of APPJ for

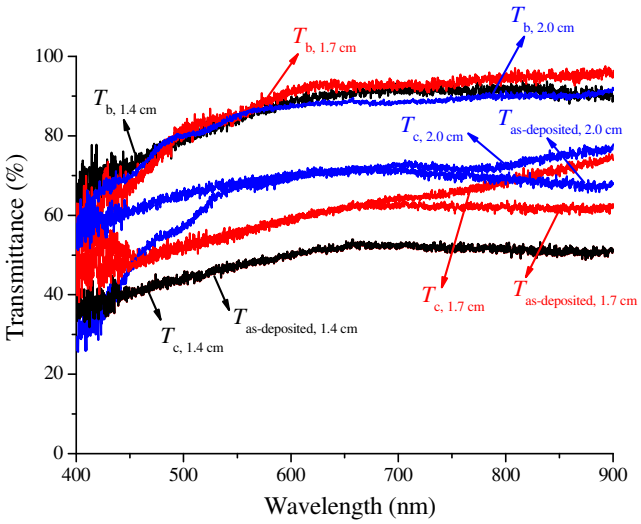

Fig. 5 The transmittance spectra of as-deposited, the bleached, and the colored glass/ITO/NiO_xC_y after 200 cycles of Li^+ intercalation and deintercalation plotted as a function of wavelength at various substrate distances

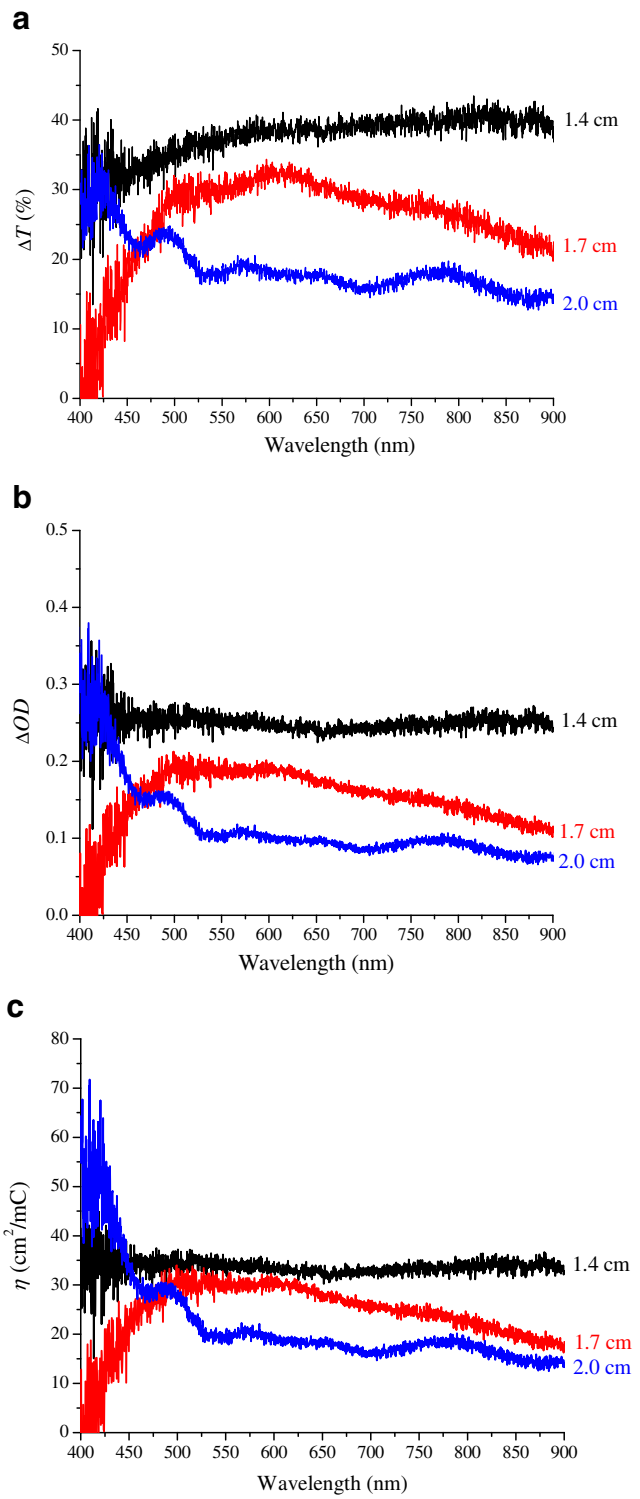

Fig. 6 **a** Transmittance variation (ΔT), **b** optical density change (ΔOD), and **c** color efficiency (η) of glass/ITO/NiO_xC_y after 200 cycles of Li^+ intercalation and deintercalation plotted as a function of wavelength at various substrate distances

Table 4 Atomic compositions of NiO_xC_y films at various substrate distances

L (cm)	1.4	1.7	2.0
Ni (%)	11.9±1.2	15.5±1.6	20.1±2.0
O (%)	40.7±4.1	31.2±3.1	39.0±3.9
C (%)	47.4±4.7	53.2±5.3	40.9±4.1

synthesis of NiO_xC_y thin films, the higher the transmittance variation ΔT, the optical density change ΔOD, and the color efficiency η for the wavelengths of 450–900 nm.

Optical properties of NiO_x films in low light modulation values are questioned for using in devices while the optical modulation depends on Li^+ ion transport [1]. Newly, light modulation in transmittance variation ΔT up to 15% is examined in 300-nm-thick NiO_x films deposited onto glass/ITO by d.c. sputtering from metallic Ni target at a power of 250 W in argon/oxygen atmosphere with an O_2/Ar mass flow rate of 2% [23]. Although PECVD can offer higher deposition rates than reactive sputter deposition [10], electrochromic nickel oxide thin films have not yet synthesized by PECVD. In this study, rapid deposition (i.e., short durations of 21–28 s exposed in plasma torch) of 252–262-nm-thick electrochromic NiO_xC_y thin films onto glass/ITO by AP-PECVD with APPJ has been elucidated. Velevska and Ristova [24] report a transmittance variation ΔT of up to 40% in a 0.1-M NaOH aqueous electrolyte for nickel oxide films evaporated onto glass/ITO. Therefore, this study accomplishes an notable transmittance variation ΔT of up to 43% for APPJ-synthesized NiO_xC_y thin films onto glass/ITO even after 200 cycles of Li^+ intercalation and deintercalation.

Surface composition dependence

The atomic compositions of Ni, O, and C in NiO_xC_y thin films can be calculated from the intensity area of XPS spectra of Ni_{2p}, O_{1s}, and C_{1s}. The atomic compositions of N for APPJ-synthesized NiO_xC_y thin films are found to be less than 0.06%, which is negligible in this study. Table 4 shows the atomic compositions of APPJ-synthesized NiO_xC_y films at various substrate distances. The lower substrate distance at 1.4 cm for synthesis, the lower content of nickel at 11.9%, and the higher content of oxygen at 40.7% are produced. Table 5 reveals that the lower the substrate distances are applied, the higher the O/Ni ratios (x values) and C/Ni ratios (y values) in APPJ-synthesized NiO_xC_y films are obtained. The ratios of O/Ni (x value) and C/Ni (y value) in APPJ-synthesized NiO_xC_y films are 1.94–3.42 and 2.03–3.98, respectively. In this study, the carbon in precursor [nickelocene, $Ni(C_5H_5)_2$] is used to assist Ni and O synthesizing NiO_xC_y thin film. It can be proven by the higher deposition rate (see Table 2) for deposition of NiO_xC_y thin film at the substrate distance of 1.4 cm resulting in the higher ratios of oxygen to nickel (i.e., the x value) and carbon to nickel (i.e., the y value) in NiO_xC_y thin film. However, the higher y values in NiO_xC_y thin films cause the lower transmittances (see Fig. 5) of the as-deposited NiO_xC_y thin films.

Valence changes in Ni ion between Ni^{2+} of NiO (colorless) and Ni^{3+} of Ni_2O_3 (dark brown) are proposed as the reason for the color change as is the case with alkaline electrolyte [3]. As Li^+ ions and electrons flow into the NiO_xC_y thin film, some Ni^{3+} ions are reduced to Ni^{2+} and polarize their surrounding lattice to form small polarons. Optical absorption is caused by small polaron transitions between two adjacent non-equivalent sites of nickel ions (Ni^{2+} and Ni^{3+}) (8):

$$h\nu + Ni^{2+}(A) + Ni^{3+}(B) \rightarrow Ni^{3+}(A) + Ni^{2+}(B) \quad (8)$$

To determine the proportions of Ni^{2+} and Ni^{3+} on the surface of APPJ-synthesized NiO_xC_y thin film, the XPS spectra of Ni_{2p}, O_{1s}, and C_{1s} in Fig. 7a–c are fitted after subtraction of Shirley background using Lorentzian (80%)–Gaussian (20%) product functions with full width at half maxima of 2 eV. The binding energies of the main doublet $Ni^{2+}_{2p3/2}$ and $Ni^{3+}_{2p3/2}$ for the Ni^{2+} and Ni^{3+} core-level spectra of NiO and Ni_2O_3 are 854.5 and 856.5 eV, respectively. The

Table 5 x and y values of NiO_xC_y, x_1 and x_2 values of $NiO_{x_1}C_yO_{x_2}$, and z value of $Ni_{1-z}O$

L (cm)			1.4	1.7	2.0
NiO_xC_y	x		3.42±0.34	2.01±0.20	1.94±0.19
	y		3.98±0.40	3.43±0.34	2.03±0.20
$NiO_{x_1}(C-C)_{(y-x_2)/2}$ $(C-O)_{x_{2a}}(C=O)_{x_{2b}}$	x_1		1.27±0.13	1.22±0.12	1.19±0.12
	$x_2 = x_{2a} + x_{2b}$	x_{2a} (C–O)	0.93±0.09	0.43±0.04	0.38±0.04
		x_{2b} (C=O)	1.21±0.12	0.36±0.04	0.37±0.04
	$(y–x_2)/2$ (C–C)		0.92±0.09	1.32±0.13	0.64±0.06
$Ni_{1-z}O$	z		0.21±0.02	0.18±0.02	0.16±0.02

x_1 value in $NiO_{x_1}C_yO_{x_2}$ films can be found by taking the arithmetic average of the proportions of Ni_2O_3 (Ni^{3+}) for 1.5 and NiO (Ni^{2+}) for 1, respectively, as shown in Table 5. The x_2 value of $NiO_{x_1}C_yO_{x_2}$ films can be calculated by $x_2 = x - x_2$. The x_2 value can be referred to as the cumulated proportions of chemical bonds C–O and C=O, as shown in Fig. 7b, c. Then, the $(y-x_2)/2$ value for $NiO_{x_1}C_yO_{x_2}$ films can be referred to as the proportion of chemical bond C–C. The x_{2a} and x_{2b} values in x_2 values can be referred to as the proportions of chemical bonds C–O and C=O.

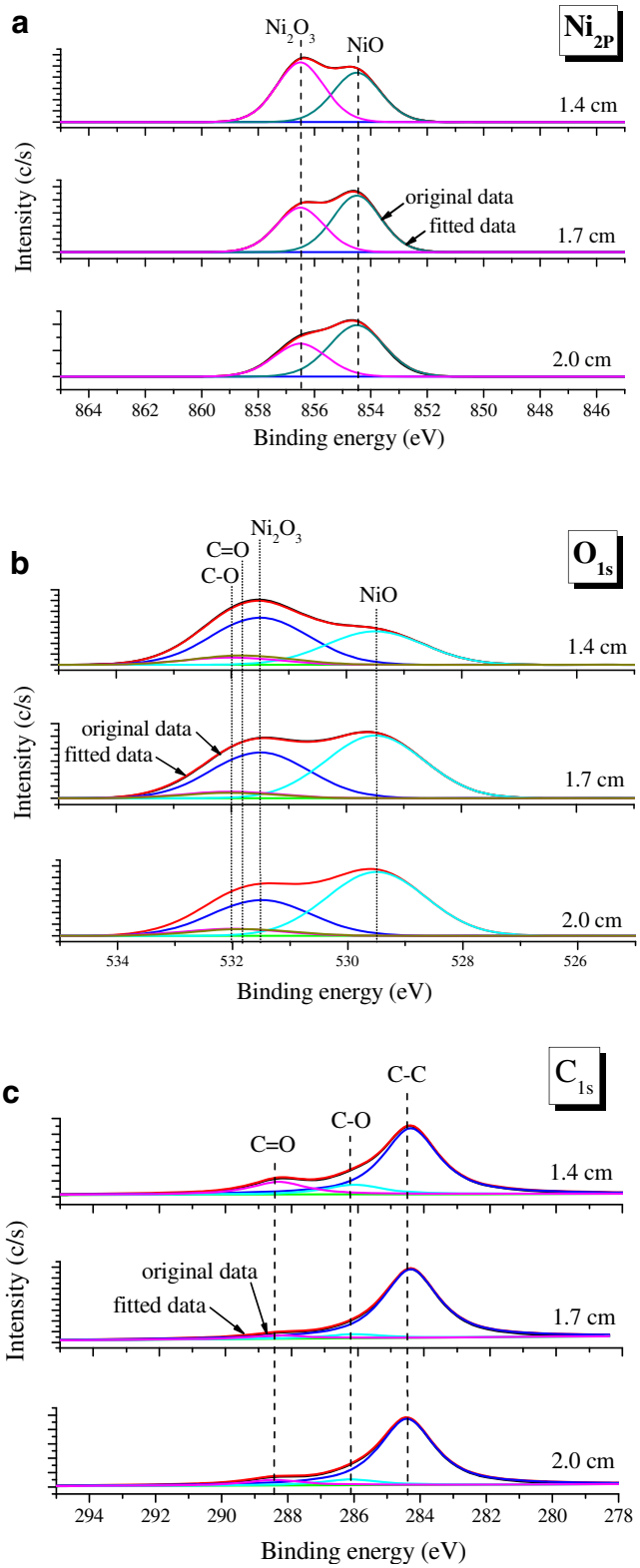

Fig. 7 **a** Ni_{2p}, **b** O_{1s}, and **c** C_{1s} spectra of glass/ITO/NiO_xC_y at various substrate distances plotted as a function of binding energies

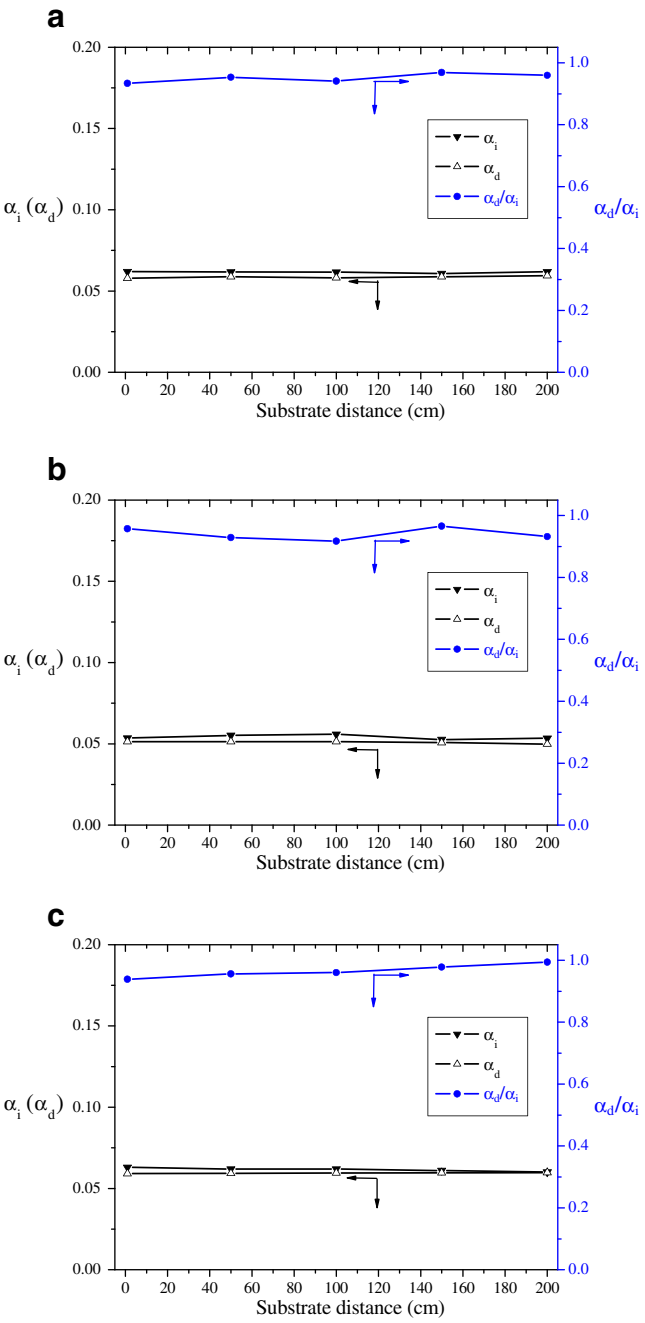

Fig. 8 α_i, α_d, and α_d/α_i (reversibility) of glass/ITO/NiO_xC_y after 1–200 cycles of Li^+ intercalation and deintercalation for substrate distances of **a** 1.4 cm, **b** 1.7 cm, and **c** 2.0 cm

To find the theoretical vacancy for Li^+ intercalation into $NiO_{x_1}C_yO_{x_2}$ thin film, NiO_{x_1} in $NiO_{x_1}C_yO_{x_2}$ thin film is denoted as $Ni_{1-z}O$. The fraction of Ni_2O_3 in $Ni_{1-z}O$ is dependent on the z value. The value of z is referred to as the fraction of Ni_2O_3 in $Ni_{1-z}O$ film, i.e., the theoretical vacancy in $NiO_{x_1}C_yO_{x_2}$ film for double intercalation with the electron (e^-) supplied by electrochemical station at work electrode (cathode) and Li^+ ion offered from 1 M $LiClO_4$–PC electrolyte. The z values of $Ni_{1-z}O$ films are 0.16–0.21 at various substrate distances, as shown in Table 5. Figure 8a–c shows that the intercalation coefficient (α_i) and deintercalation coefficient (α_d) of $Ni_{1-z}O$ film for 1–200 cycles of Li^+ intercalation/deintercalation from −0.5 to 1.5 V are 0.0608–0.0620 and 0.0579–0.0594 for substrate distance at 1.4 cm, 0.0608–0.0620 and 0.0579–0.0694 for substrate distance at 1.7 cm, and 0.0526–0.0559 and 0.0498–0.0513 for substrate distance at 2.0 cm, respectively. The α_i and α_d are much lower than the theoretical vacancy in NiO_{x_1} film for keeping a reversible Li^+ intercalation/deintercalation. Therefore, the high α_d/α_i (reversibility) values for glass/ITO/NiO_xC_y films after 1–200 cycles of CV measurements at substrate distances of 1.4, 1.7, and 2.0 cm are achieved for 0.9339–0.9688, 0.9317–0.9654, and 0.9388–0.9942, respectively. Table 5 indicates that the lower the substrate distance for APPJ-synthesized NiO_xC_y films, the higher the z values in NiO_xC_y films. The higher the z values in NiO_xC_y films not only indicate the more the brown color as referred to as the lower transmittances of the colored glass/ITO/NiO_xC_y but also the higher the number of sites available for electron and Li^+ double insertions into NiO_xC_y films, resulting more Li^+ intercalation into APPJ-synthesized NiO_xC_y films and the higher transmittances of the bleached glass/ITO/NiO_xC_y even after 200 cycles of CV measurements, as shown in Fig. 5.

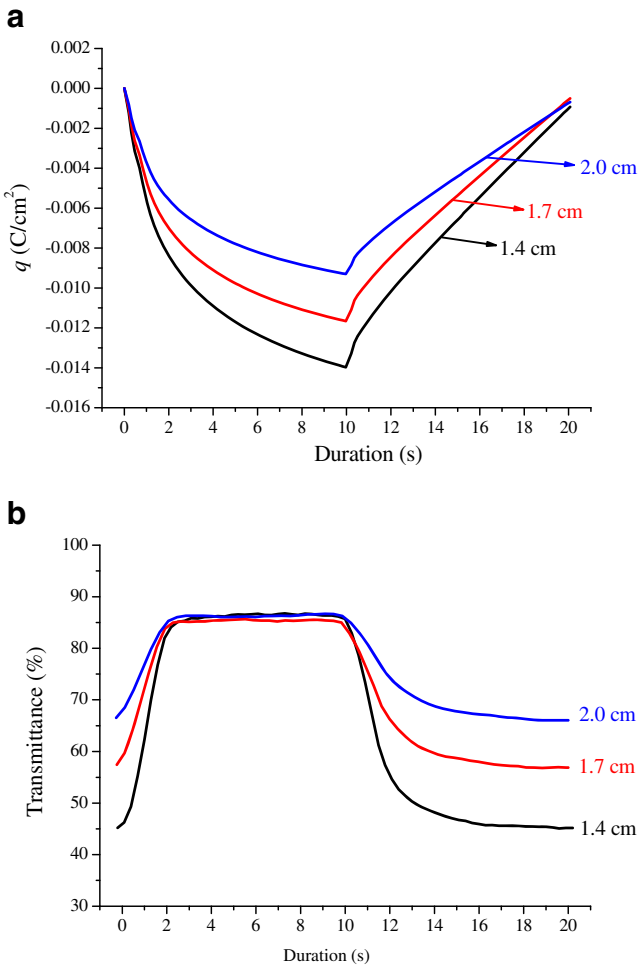

Fig. 9 Responses in **a** charges per unit area and **b** transmittances at a wavelength of 550 nm for glass/ITO/NiO_xC_y prepared at various substrate distances and after 200 cycles of Li^+ intercalation and deintercalation

Potential step in situ electrochromic behavior

Figure 9a indicates that the lower the substrate distance (1.4 cm) for APPJ-synthesized NiO_xC_y films, the higher the Li^+ charge intercalation/deintercalation per unit area q (14 mC/cm^2). The lower substrate distance at 1.4 sccm from the nozzle of APPJ results in a fast bleaching at −0.5 V for 2 s and a fast coloration at +1.5 V for 6 s even after 200 cycles of CV measurements, as shown in Fig. 9b.

Conclusions

Rapid deposition of significant electrochromic organonickel oxide (NiO_xC_y) thin films onto the moving glass/ITO substrates by a short duration of 21 s has been demonstrated by injection of precursor NO vapor into the air plasma torch of APPJ at a substrate distance of 1.4 cm. NiO_xC_y thin films with nano-porous surfaces and high vacancies for Li^+ intercalation are produced. The high grain boundary fractions between nano-particles in NiO_xC_y thin films allow Li^+ to be intercalated into and deintercalated out from NiO_xC_y thin films easily, which results in a reversibly fast bleaching at −0.5 V for 2 s and a reversibly fast coloration at +1.5 V for 6 s for 200 cycles of potential step measurements in a 1-M $LiClO_4$–PC electrolyte. The high fraction of Ni_2O_3 in organonickel oxide thin films provides a significant transmittance variation of 43% at a wavelength of 830 nm after 200 cycles of reversible Li^+ intercalation and deintercalation.

Acknowledgments This study is supported by the National Science Council of the Republic of China (NSC99-2221-E-035-086 and NSC100-2221-E-035-059).

References

1. Niklasson GA, Granqvist CG (2007) J Mater Chem 17:127–156
2. Cordoba-Torresi SI, Goff AH, Joiret S (1991) J Electrochem Soc 138:1554–1559
3. Passerini S, Scrosati B, Gorenstein A (1990) J Electrochem Soc 137:3297–3300
4. Ozkan Zayim E, Turhan I, Tepehan FZ, Ozer N (2008) Sol Energy Mater Sol Cells 92:164–169
5. Uplane MM, Mujawar SH, Inamdar AI, Shinde PS, Sonavane AC, Patil PS (2007) Appl Surf Sci 253:9365–9371
6. Kamal H, Elmaghraby EK, Ali SA, Abdel-Hady K (2005) Thin Solid Films 483:330–339
7. Porqueras I, Bertran E (2001) Thin Solid Films 398–399:41–44
8. Lin YS, Chen PW, Lin DJ, Chuang PY, Tsai TH, Shiah YC, Yu YC (2010) Surf Coat Technol 205:S216–S221
9. Wen SJ, Kerr J, Rubin M, Slack J, von Rottkay K (1999) Sol Energy Mater Sol Cells 56:299–307
10. Garg D, Henderson PB, Hollingsworth RE, Jensen DG (2005) Mater Sci Eng B 119:224–231
11. Baba Ali E, Berede JC, Guyomard P (2002) Thin Solid Films 402:215–221
12. Lin YS, Liu HM, Chen CL (2006) Surf Coat Technol 200:3775–3785
13. Estrada W, Andersson AM, Granqvis CGt (1988) J Appl Phys 64:3678
14. Wruck DA, Dixon MA, Rubin M, Bogy SN (1991) J Vacuum Sci Technol A 9:2170–2173
15. Mariotti D, Sankaran RM (2010) J Phys D 43:323001
16. Borra JP (2006) J Phys D 39:R19–R54
17. Mariotti D, Ostrikov K (2009) J Phys D 42:092002
18. Lee SH, Cheong HM, Park NG, Tracy CE (2001) Solid State Ionics 140:135–139
19. Das A, Chakraborty B, Sood AK (2008) B Mater Sci 31:579–584
20. Lo YL, Hwang BJ (1998) Langmuir 14:944–950
21. Melendres CA, Xu S (1984) J Electrochem Soc 131:2239–2243
22. Parker SF, Williams KPJ, Smith T, Bortz M, Bertheville B, Yvon K (2002) Phys Chem Chem Phys 4:1732–1737
23. Green S, Backholm J, Georen P, Granqvist CG, Niklasson GA (2009) Sol Energy Mater Sol Cells 93:2050–2055
24. Velevska J, Ristova M (2002) Sol Energy Mater Sol Cells 73:131–139